Chemical Methodologies 7(2023) 248-256

Chemical Methodologies

Journal homepage: http://chemmethod.com

Original Research Article

Investigation of Adsorption Properties of $Al_{12}N_{12}$, $SiAl_{11}N_{12}$, and GaAl11N12 Nanoclusters for Sarin Detection: A Comparative DFT Study

Mahdi Mohammad Alizadeh, Farshid Salimi*, Gholamreza Ebrahimzadeh-Rajaei**

Department of Chemistry, Ardabil Branch, Islamic Azad University, Ardabil, Iran

ARTICLE INFO

Article history

Submitted: 2022-10-19
Revised: 2022-11-05
Accepted: 2022-12-12
Manuscript ID: CHEMM-2211-1628
Checked for Plagiarism: Yes
Language Editor:
Dr. Fatimah Ramezani
Editor who approved publication:
Dr. Mohsen Oftadeh

DOI:10.22034/CHEMM.2023.370868.1628

KEYWORDS

$Al_{12}N_{12}$ nanoclusters
Sensor
DFT
Sarin
Adsorption

ABSTRACT

In this study, the capability to adsorb and detect of pure and doped $Al_{12}N_{12}$ nanoclusters were utilized to detect sarin nerve agents using the density functional theory (DFT) calculation. After adsorption of sarin on the $Al_{12}N_{12}$, $SiAl_{11}N_{12}$, and $GaAl_{11}N_{12}$ nanoclusters, the adsorption energies (E_{ad}) were calculated at -38.36, -25.95, and -27.94 kcal mol^{-1}, respectively. The electrical properties calculations indicated electrical conductivity changes after adsorption of sarin are -3.04%, -24.64%, and -1.16% for $Al_{12}N_{12}$, $SiAl_{11}N_{12}$, and $GaAl_{11}N_{12}$, respectively. Thus, it is clear that the $SiAl_{11}N_{12}$ nanocluster demonstrated a considerable change in the electrical conductivity, and these changes could be considered as the signal for the sarin detection. Moreover, $SiAl_{11}N_{12}$ indicated an ideal recovery time for sarin desorption from nanoclusters. Thus, it can be concluded that the $SiAl_{11}N_{12}$ nanocluster is an appropriate candidate for the sarin detection.

GRAPHICAL ABSTRACT

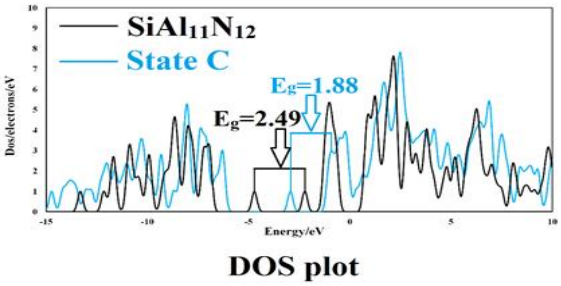

DOS plot

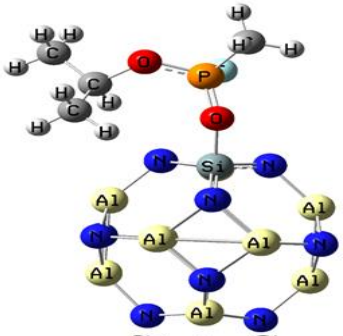

State C

* Corresponding author: Farshid Salimi
✉ E-mail: Salimi982020@gmail.com
** Co-Corresponding author: Gholamreza Ebrahimzadeh-Rajaei
✉ E-mail: gh_rajaei@iauardabil.ac.ir

Introduction

Of the chemical warfare agents, the nerve agent is the most hazardous [1]. They influence fast on human health and lead to death [2, 3]. Sarin, as a dangerous nerve agent, is a potent acetylcholinesterase inhibitor [4]. Due to be odorless, tasteless, and colorless detection of sarin is very hard [5]. Thus, designing a reliable and facile technique for the sarin detection is highly essential.

For sarin detection, several techniques, such as chromatography [6], photo luminescent [7], mass spectroscopy [8], and fluorescent sensors [9] have been utilized. Nevertheless, these techniques need more energy and time and are expensive. Compared with these techniques, chemical sensors based on the nanostructures have been used widely due to their short response time, high selectivity, affordable, and comfortable applications [10-15]. Thus, nanoclusters have recently been considered as an alternative approach to the chemical sensors [16-21]. Among different kinds of nanoclusters, aluminum nitride (AlN) nanostructures were extensively used due to the wide bandgap, economic efficiency, and thermal stability [22-24].

The AlN nanostructures could be modified by loading noble metals and doping atomic impurities [25-29]. For example, Nayini *et al.* investigated the sensitivity and reactivity of pure and Si-, Ga-, and Ge-doped AlN nanoclusters with amphetamine drugs using density functional theory (DFT) calculations [26]. They indicated that Si-doped AlN is a potential nanocluster for the amphetamine detection. Thus, in this study, we investigated the adsorption and detection properties of sarin on the $Al_{12}N_{12}$, Si-doped AlN ($SiAl_{11}N_{12}$), and Ga-doped AlN ($GaAl_{11}N_{12}$) nanoclusters using the DFT calculations.

Computational method

The sarin interaction with the $Al_{12}N_{12}$, $SiAl_{11}N_{12}$, and $GaAl_{11}N_{12}$ nanoclusters surfaces was calculated using the DFT calculations. The GAMESS program [30] and the M06 method with an and 6-311G (d, P) basis set were utilized for all investigations. Reports indicated that the M06 method is very reliable due to the excellent agreement with the experimental results. The previous reports have indicated that the M06 method is better than the other methods, such as B3LYP, MP2, B9W91, QCISD, and QCISD (T) [31, 32]. 6-311G (d, p) basis set has been known suitable for nanostructure systems [33, 34]. The adsorption energies (E_{ad}) of sarin onto the $Al_{12}N_{12}$, $SiAl_{11}N_{12}$, and $GaAl_{11}N_{12}$ nanoclusters are as follow:

$$E_{ad}=E(sarin/Al_{12}N_{12})-E(Al_{12}N_{12})-E(sarin) \quad (1)$$

$$E_{ad}=E(sarin/SiAl_{11}N_{12})-E(SiAl_{11}N_{12})-E(sarin) \quad (2)$$

$$E_{ad}=E(sarin/GaAl_{11}N_{12})-E(GaAl_{11}N_{12})-E(sarin) \quad (3)$$

Where, $E(sarin/Al_{12}N_{12})$, $E(sarin/SiAl_{11}N_{12})$, and $E(sarin/GaAl_{11}N_{12})$ are the total energies of the sarin interacted $Al_{12}N_{12}$, $SiAl_{11}N_{12}$, and $GaAl_{11}N_{12}$ nanoclusters, respectively. E(sarin), $E(Al_{12}N_{12})$, $E(SiAl_{11}N_{12})$, and $E(GaAl_{11}N_{12})$ are the total energy of pristine sarin, $Al_{12}N_{12}$, $SiAl_{11}N_{12}$, and $GaAl_{11}N_{12}$, respectively.

Results and Discussion

Adsorption of sarin on $Al_{12}N_{12}$

The molecular electrostatic potential (MEP) plot of sarin in Figure 1 indicated fluorine (F) and carbonyl oxygen atoms have a more negative charge (red color) and make it an electronegative site for interaction with the electrophilic region.

Figure 1 demonstrated the most stable structure of $Al_{12}N_{12}$ with six-membered (6-R) and four-membered (4-R) rings. The bond lengths of the 6R-4R and 6R-6R mutual bonds of Al-N atoms were calculated at 1.84 and 1.78 Å, which is consistent with previous reports [35]. The MEP plot of $Al_{12}N_{12}$ was shown that the Al and N atoms are electrophilic (blue color) and nucleophile (red color) regions, respectively. To investigate the adsorption properties of sarin with nanoclusters, various possible adsorption sites of sarin (F and carbonyl oxygen atoms) were considered for the interaction with $Al_{12}N_{12}$ nanoclusters. After optimization, the adsorption energy and bound distance between the nanocluster and sarin from its carbonyl oxygen atom (state A) were calculated at -38.36 kcal.mol-

[1] and 1.89 Å, which indicated an appropriate interaction. The sarin adsorption from its F atom was calculated in state B (Figure 2). Adsorption energies in state B were investigated at -20.62 kcal.mol^{-1}, and equilibrium distances were 2.97 Å (Table 1). Therefore, these parameters demonstrated the adsorption of sarin from its carbonyl oxygen atom (state A) is stronger since the equilibrium distance between sarin and the $Al_{12}N_{12}$ nanocluster was shorter and the adsorption energy was more negative. The AlN nanocluster dipole moment (DM) value increased after the adsorption of sarin from 0.00 Debye in pure $Al_{12}N_{12}$ to 8.79 and 3.70 Debye, representing polar bonds between nanocluster and sarin.

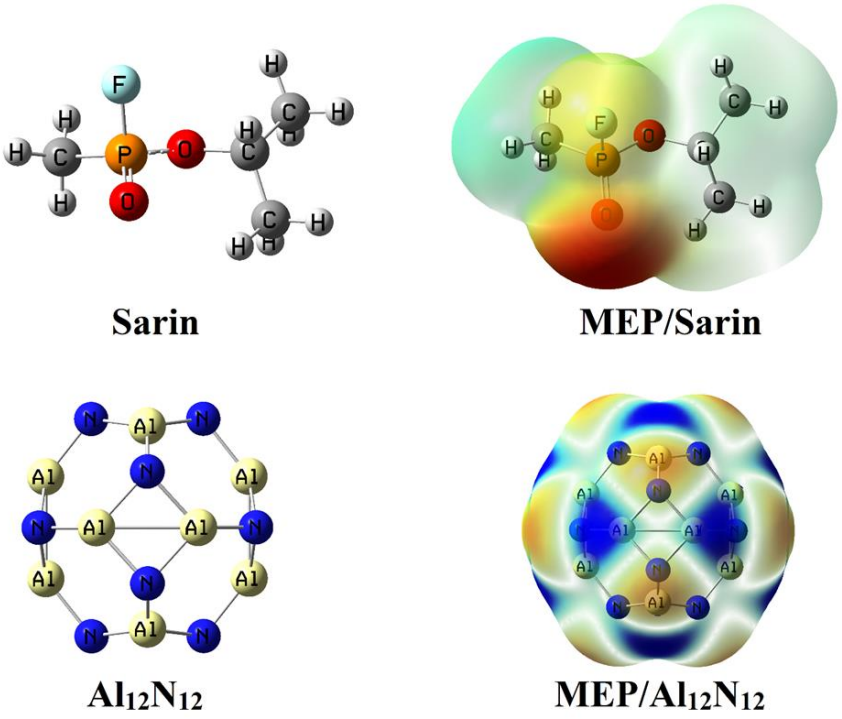

Figure 1: The optimized structures and MEP plot for the sarin and $Al_{12}N_{12}$

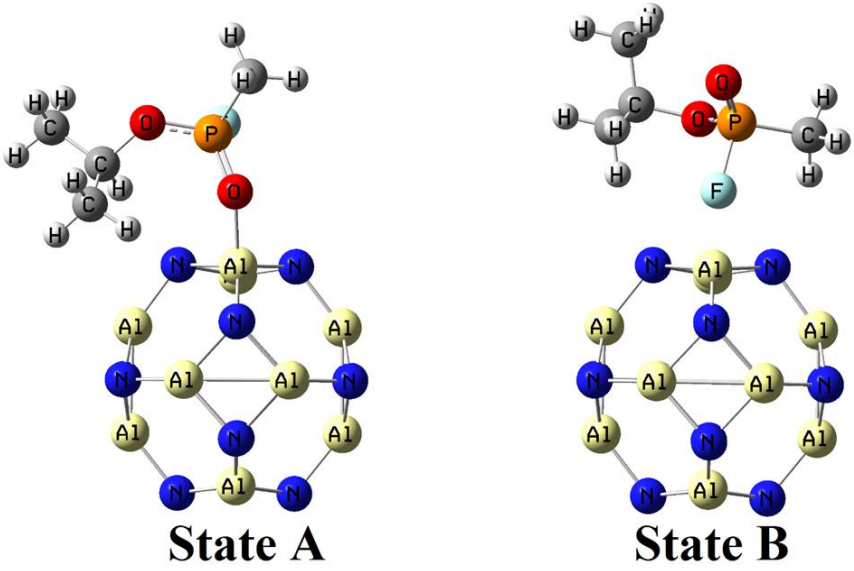

Figure 2: The optimized configurations for the $Al_{12}N_{12}$ complexes in different states

Table 1: The calculated adsorption energy (E_{ad}), bond distance between sarin and nanoclusters (D), HOMO energy (E_{HOMO}), LUMO energy (E_{LUMO}), energy gap (E_g), electrical conductivity variation (%Δσ) after the sarin adsorption, and dipole moment (DM) in gas phase

Name	E_{ad} (kcal mol^{-1})	D (Å)	E_{HOMO} (eV)	E_{LUMO} (eV)	E_g (eV)	%Δσ	DM (Debye)
Sarin	-	-	-8.61	0.88	9.49	-	3.03
$Al_{12}N_{12}$	-	-	-6.80	-2.23	4.57	-	0.00
A	-38.36	1.89	-6.13	-1.70	4.43	-3.04	8.79
B	-20.62	2.97	-6.51	-2.00	4.51	-1.31	3.70
$SiAl_{11}N_{12}$	-	-	-4.71	-2.22	2.49	-	1.61
C	-25.95	1.82	-2.93	-1.05	1.88	-24.64	12.81
D	-3.71	2.24	-3.34	-1.46	1.89	-24.1	7.06
$GaAl_{11}N_{12}$	-	-	-6.79	-2.34	4.46	-	0.67
E	-27.94	2.02	-6.22	-1.82	4.40	-1.16	7.49
F	-12.47	2.25	-6.53	-2.05	4.48	0.45	4.13

Adsorption of sarin on the $SiAl_{11}N_{12}$ and $GaAl_{11}N_{12}$ nanoclusters

To investigate the doping effect on the adsorption process, Si and Ga atoms were doped into the $Al_{12}N_{12}$ nanocluster (Figure 3). The previous reports indicated Si and Ga atoms could be doped in the AlN nanoclusters [26]. The Si-O and Ga-O bond lengths in the 6R-4R and 6R-6R mutual bonds indicated a bond length of 1.84 and 1.78 Å, which is consistent with reports [36, 37].

After the sarin adsorption on the $SiAl_{11}N_{12}$, adsorption energies (equilibrium distances) were calculated at -25.95 (1.82 Å) and -3.71 kcal.mol^{-1} (2.24 Å) in states C and D (Figure 4). The adsorption energies for $GaAl_{11}N_{12}$ in states E and F were investigated at -27.94 and -12.47 kcal.mol^{-1}, respectively, and the equilibrium distances were calculated at about 2.02 and 2.25 Å. These values indicated similar to the $Al_{12}N_{12}$ adsorption of sarin from its carbonyl oxygen atom is stronger than the other states, and this orientation was the most stable state. The NBO charge transfers calculation indicated charge transfer from sarin to the nanoclusters. The DM values in Table 1 indicated that after the sarin adsorption on the $SiAl_{11}N_{12}$ and $GaAl_{11}N_{12}$, the values increase.

Electronic characteristics before and after interactions of nanoclusters

In Table 1, the electronic characteristics (HOMO, LUMO, and energy gap (E_g)) of pure and complexes of nanoclusters were provided. The HOMO and LUMO energies of $Al_{12}N_{12}$ were calculated at -6.80 and -2.23 eV. Thus, the E_g energy (LUMO-HOMO) will equal 4.57 eV. Hoseininezhad-Namin *et al.* calculated the HOMO, LUMO, and E_g values of $Al_{12}N_{12}$ at -8.54, -0.63, and 7.91 eV, respectively, at the wB97XD method and 6-311G (d, p) basis set [38]. After doping Si and Ga atoms, the HOMO and LUMO values were changed. Furthermore, E_g values after the doping process reduced -45.51% and -2.45% in the $SiAl_{11}N_{12}$ and $GaAl_{11}N_{12}$ nanoclusters, respectively. Based on the previous experimental studies, the change in the sensor's signals is due to the electrical conductivity (σ) alteration after adsorption.

A shift in the electronic properties of AlN nanoclusters could change the electrical conductivity of these nanoclusters, as shown by the following equation with E_g:

$$\sigma \propto \exp \frac{-Eg}{2K_B T} \qquad (4)$$

Where, T and K_B are the temperature and Boltzmann constant, respectively. According to Equation (4), when E_g decreases after adsorption of sarin, the electrical conductivity increases. This ratio of changes could be investigated by equation (5):

$$\Delta\sigma = \frac{\sigma - \sigma_o}{\sigma_o} \qquad (5)$$

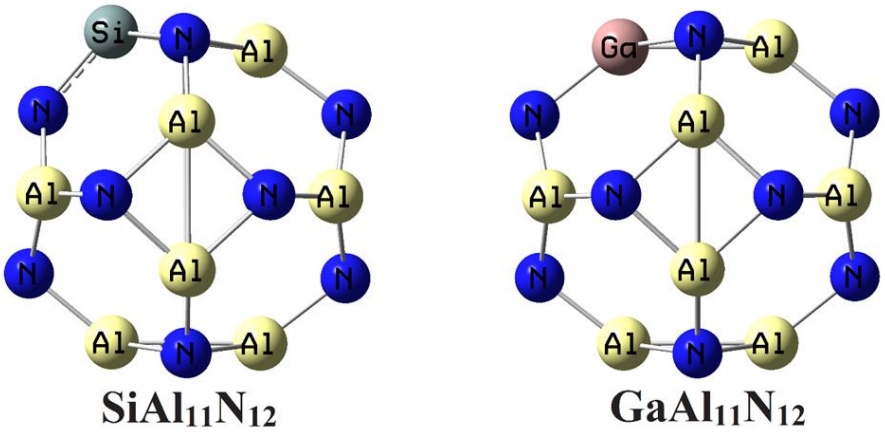

Figure 3: The optimized structures for the $SiAl_{11}N_{12}$ and $GaAl_{11}N_{12}$ nanostructures

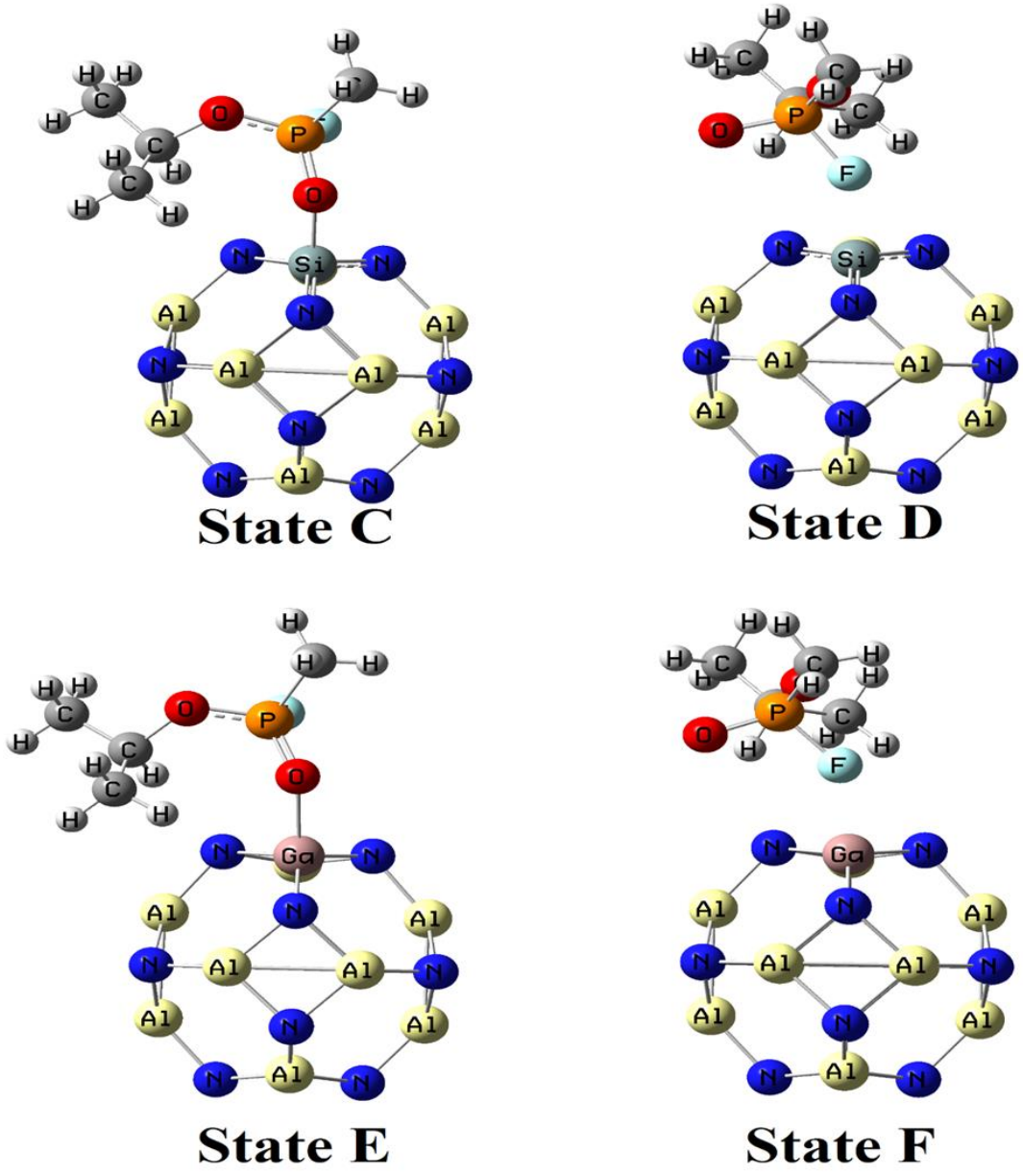

Figure 4: The optimized configurations for the $SiAl_{11}N_{12}$, and $GaAl_{11}N_{12}$ complexes in different states

Where, σ_0 and σ are the electrical conductivity of pure nanoclusters and complexes, respectively. The $\%\Delta\sigma$ shows the signal strength, corroborating the sarin's existence. As indicated in Table 1, the $\%\Delta\sigma$ after the interaction of nanoclusters with sarin is -3.04%, -24.64%, and -1.16% for $Al_{12}N_{12}$, $SiAl_{11}N_{12}$, and $GaAl_{11}N_{12}$, respectively, in the most stable states. Thus, it is clear that $SiAl_{11}N_{12}$ has higher performance for sarin detection than $Al_{12}N_{12}$ and $GaAl_{11}N_{12}$. DOS and MEP plots of the $SiAl_{11}N_{12}$ complex are indicated in Figure 5. As displayed in Figure 5, after the sarin interaction with $SiAl_{11}N_{12}$, the DOS plots were changed in HOMO and LUMO energy levels and changed to the lower energies. Thus, the HOMO and LUMO energies stabilized after adsorption and altered the E_g region. MEP plot of the $SiAl_{11}N_{12}$ complex in Figure 5 demonstrated the significant change in the electrostatic potential after the interaction. This Figure indicated that sarin is more positive (blue and green colors) after the adsorption processes. Therefore, these results demonstrated charge transfers from sarin to the $SiAl_{11}N_{12}$ nanoclusters, which confirm the charge transfer values.

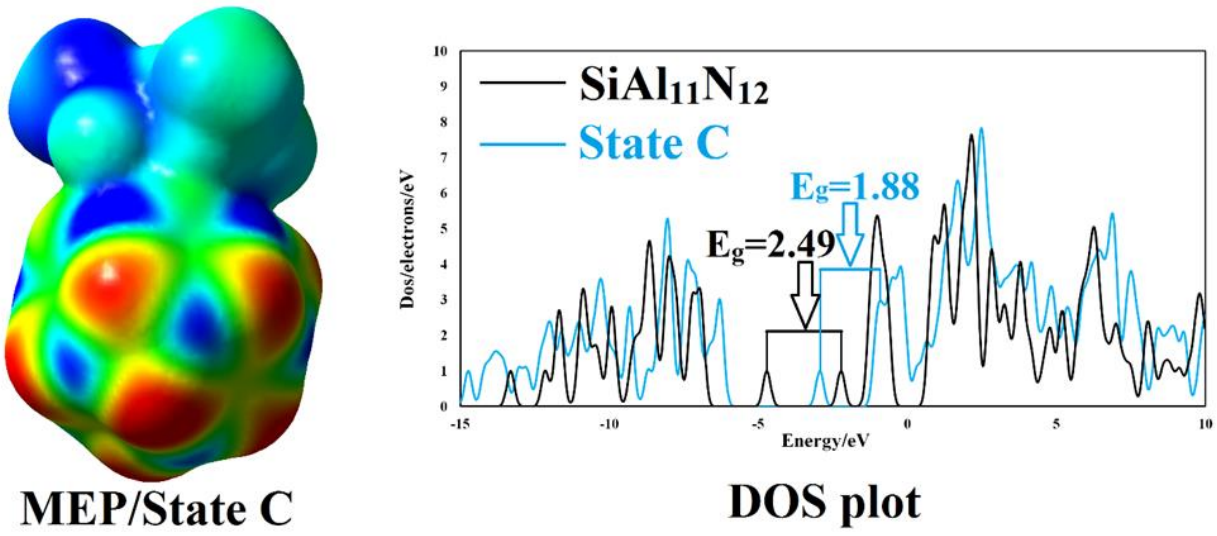

Figure 5: DOS and MEP plots of sarin/$SiAl_{11}N_{12}$ (state C)

Recovery time

The interaction strength is essential in developing sensors because a strong adsorption leads to the long-term desorption, and thereby increasing the recovery time. In experimental studies, sensor recovery time can be calculated through methods including heating or exposure to the UV light [39]. Thus, the recovery time could be investigated from the following equation:

$$\tau = \upsilon^{-1}\exp\left(\frac{E_{ad}}{KT}\right) \qquad (6)$$

Where, T is the temperature, k is the Boltzmann's constant, and ν indicates UV frequency. Therefore, the recovery time for $Al_{12}N_{12}$, $SiAl_{11}N_{12}$, and $GaAl_{11}N_{12}$ complexes will be about 12.37×10^9, 9.93, and 284.68 s at the UV frequency of 10^{18} s^{-1} and 298 K, respectively. These values showed that $Al_{12}N_{12}$ and $GaAl_{11}N_{12}$ have a long recovery time and long-term desorption. Thus, it could not be used for sarin detection. On the other hand, $SiAl_{11}N_{12}$ demonstrated the short-term desorption suitable for sensor applications.

Conclusion

The interaction of sarin with the $Al_{12}N_{12}$, $SiAl_{11}N_{12}$, and $GaAl_{11}N_{12}$ nanoclusters was studied using DFT calculations to explore a new system for sarin detection. After optimization, adsorption energies were calculated at -38.36, -25.95, and -27.94 kcal mol^{-1} for $Al_{12}N_{12}$, $SiAl_{11}N_{12}$, and $GaAl_{11}N_{12}$, respectively. The electrical properties calculations indicated the electrical conductivity changes after adsorption of sarin are -3.04%, -

24.64%, and -1.16% for $Al_{12}N_{12}$, $SiAl_{11}N_{12}$, and $GaAl_{11}N_{12}$, respectively. This variation can be considered as a signal of sarin detection. Thus, the $SiAl_{11}N_{12}$ nanocluster has a high sensitivity to the detection of sarin nerve agents. On the other hand, the recovery time calculation based on the transition theory confirmed that only the pristine $SiAl_{11}N_{12}$ showed a short recovery time of 9.93s s, demonstrating that sarin adsorption on that is reversible and more favorable. Therefore, it is concluded that the $SiAl_{11}N_{12}$ nanocluster can be used as a suitable sarin detector.

Acknowledgements

This article was derived from Ph.D. Degree thesis in the Islamic Azad University, Ardabil Branch.

Funding

This research did not receive any specific grant from funding agencies in the public, commercial, or not-for-profit sectors.

Authors' contributions

All authors contributed to data analysis, drafting, and revising of the paper and agreed to be responsible for all the aspects of this work.

Conflict of Interest

We have no conflicts of interest to disclose.

References

[1]. Kloske M., Witkiewicz Z., Novichoks – The A group of organophosphorus chemical warfare agents, *Chemosphere*, 2019, **221**:672 [Crossref], [Google scholar], [Publisher]

[2]. Picard B., Chataigner I., Maddaluno J., Legros J., Introduction to chemical warfare agents, relevant simulants and modern neutralisation methods, *Organic & Biomolecular Chemistry*, 2019, **17**:6528 [Crossref], [Google scholar], [Publisher]

[3]. Nepovimova E., Kuca K., Chemical warfare agent NOVICHOK - mini-review of available data, *Food and chemical toxicology*, 2018, **121**:343 [Crossref], [Google scholar], [Publisher]

[4]. Zhang S.W., Swager T.M., Fluorescent detection of chemical warfare agents: functional group specific ratiometric chemosensors, *Journal of the American Chemical Society*, 2003, **125**:3420 [Crossref], [Google scholar], [Publisher]

[5]. Singh V.V., Kaufmann K., Orozco J., Li J., Galarnyk M., Arya G., Wang J., Micromotor-based on–off fluorescence detection of sarin and soman simulants, *Chemical Communications*, 2015, **51**:11190 [Crossref], [Google scholar], [Publisher]

[6]. Stavrianidi A.N., Braun A.V., Stekolshchikova E.A., Baygildiev T.M., Rodin I.A., Rybalchenko I.V., Selection of Recording Conditions and Study of Fragmentation of a Peptide Biomarker of Sarin by High-Performance Liquid Chromatography–High-Resolution Mass Spectrometry, *Journal of Analytical Chemistry*, 2018, **73**:1357 [Crossref], [Google scholar], [Publisher]

[7]. Kim S., Cho B., Sohn H., Detection of nerve agent stimulants based on photoluminescent porous silicon interferometer, *Nanoscale research letters*, 2012, **7**:527 [Crossref], [Google scholar], [Publisher]

[8]. Zydel F., Smith J.R., Pagnotti V.S., Lawrence R.J., McEwen C.N., Capacio B.R., Rapid screening of chemical warfare nerve agent metabolites in urine by atmospheric solids analysis probe-mass spectroscopy (ASAP-MS), *Drug Testing and Analysis*, 2012, **4**:308 [Crossref], [Google scholar], [Publisher]

[9]. Dale T.J., Rebek Jr J., Fluorescent sensors for organophosphorus nerve agent mimics, *Journal of the American Chemical Society*, 2006, **128**:4500 [Crossref], [Google scholar], [Publisher]

[10]. Rad A.S., Comparison of X12Y12(X = Al, B and y = N, P) fullerene-like nanoclusters toward adsorption of dimethyl ether, *Journal of Theoretical and Computational Chemistry*, 2018, **17**:1850013 [Crossref], [Google scholar], [Publisher]

[11]. Peyghan A.A., Rastegar S.F., Hadipour N.L., DFT study of NH3 adsorption on pristine, Ni- and Si-doped graphynes, *Physics Letters A*, 2014, **378**:2184 [Crossref], [Google scholar], [Publisher]

[12]. Abbaspour-Gilandeh E., Aghaei-Hashjin M., Jahanshahi P., Hoseininezhad-Namin M.S., One-pot synthesis of pyrano[3,2-c]quinoline-2,5-dione derivatives by Fe3O4@SiO2-SO3H as an efficient

and reusable solid acid catalyst, *Monatshefte für Chemie-Chemical Monthly*, 2017, **148**:731 [Crossref], [Google scholar], [Publisher]
[13]. Rad A.S., Aghaei S.M., Aali E., Peyravi M., Study on the electronic structure of Cr- and Ni-doped fullerenes upon adsorption of adenine: A comprehensive DFT calculation, *Diamond and Related Materials*, 2017, **77**:116 [Crossref], [Google scholar], [Publisher]
[14]. Malhotra B.D., Ali M.A., Nanomaterials for Biosensors: Fundamentals and Applications, Elsevier Inc., 2017 [Google scholar]
[15]. Pargolghasemi P., Hoseininezhad-Namin M.S., Jadid A.P., Prediction of activities of BRAF (V600E) inhibitors by SW-MLR and GA-MLR methods, *Current Computer-Aided Drug Design*, 2017, **13**:249 [Crossref], [Google scholar], [Publisher]
[16]. Behmanesh A., Salimi F., Ebrahimzadeh Rajaei G., Adsorption behavior of letrozole on pure, Ge-and Si-doped C60 fullerenes: a comparative DFT study, *Monatshefte für Chemie-Chemical Monthly*, 2020, **151**:25 [Crossref], [Google scholar], [Publisher]
[17]. Kamali F., Ebrahimzadeh-Rajaei G., Mohajeri S., Shamel A., Khodadadi-Moghaddam M., A computational design of X24Y24 (X= B, Al, and Y= N, P) nanoclusters as effective drug carriers for metformin anticancer drug: A DFT insight, *Inorganic Chemistry Communications*, 2022, **141**:109527 [Crossref], [Google scholar], [Publisher]
[18]. Golipour-Chobar E., Salimi F., Ebrahimzadeh Rajaei G., Boron nitride nanocluster as a carrier for lomustine anticancer drug delivery: DFT and thermodynamics studies, *Monatshefte für Chemie-Chemical Monthly*, 2020, **151**:309 [Crossref], [Google scholar], [Publisher]
[19]. Kamali F., Ebrahimzadeh Rajaei G., Mohajeri S., Shamel A., Khodadadi-Moghaddam M., Adsorption behavior of metformin drug on the C60 and C48 nanoclusters: a comparative DFT study, *Monatshefte für Chemie-Chemical Monthly*, 2020, **151**:711 [Crossref], [Google scholar], [Publisher]
[20]. Gao W., Abrishamifar S.M., Rajaei G.E., Razavi R., Najafi M., DFT study of cyanide oxidation on surface of Ge-embedded carbon nanotube, *Chemical Physics Letters*, 2018, **695**:44 [Crossref], [Google scholar], [Publisher]
[21]. Karjabad K.D., Mohajeri S., Shamel A., Khodadadi-Moghaddam M., Rajaei G., Boron nitride nanoclusters as a sensor for Cyclosarin nerve agent: DFT and thermodynamics studies, *SN Applied Sciences*, 2020, **2**:574 [Crossref], [Google scholar], [Publisher]
[22]. Liu W.G., Chen G.H., Huang X.C., Wu D., Yu Y.P., DFT studies on the interaction of an open-ended single-walled aluminum nitride nanotube (AlNNT) with gas molecules, *The Journal of Physical Chemistry C*, 2012, **116**:4957 [Crossref], [Google scholar], [Publisher]
[23]. Ma Y., Huo K., Wu Q., Lu Y., Hu Y., Hu Z., Chen Y., Self-templated synthesis of polycrystalline hollow aluminium nitride nanospheres, *Journal of Materials Chemistry*, 2006, **16**:2834 [Crossref], [Google scholar], [Publisher]
[24]. Zhang X., Tang Y., Zhang F., Lee C.S., A Novel Aluminum–Graphite Dual-Ion Battery, *Advanced energy materials*, 2016, **6**:1502588 [Crossref], [Google scholar], [Publisher]
[25]. Louis H., Mathias G.E., Ikenyirimba O.J., Unimuke T.O., Etiese D., Adeyinka A.S., Metal-Doped Al12N12X (X = Na, Mg, K) Nanoclusters as Nanosensors for Carboplatin: Insight from First-Principles Computation, *The Journal of Physical Chemistry B*, 2022, **126**:5066 [Crossref], [Google scholar], [Publisher]
[26]. Nayini M.M.R., Sayadian H., Razavipour N., Rezazade M., Chemical-sensing of Amphetamine drug by inorganic AlN nano-cage: A DFT/TDDFT study, *Inorganic Chemistry Communications*, 2020, **121**:108237 [Crossref], [Google scholar], [Publisher]
[27]. Liu Q.L., Tanaka T., Hu J.Q., Xu F.F., Sekiguchi T., Green emission from c-axis oriented AlN nanorods doped with Tb, *Applied physics letters*, 2003, **83**:4939 [Crossref], [Google scholar], [Publisher]
[28]. J.S. Harris, J.N. Baker, B.E. Gaddy, I. Bryan, Z. Bryan, K.J. Mirrielees, P. Reddy, R. Collazo, Z. Sitar, D.L. Irving, On compensation in Si-doped AlN, *Applied Physics Letters*, 2018, **112**:152101 [Crossref], [Google scholar], [Publisher]
[29]. Taniyasu Y., Kasu M., Kobayashi N., Intentional control of n-type conduction for Si-

doped AlN and Al XGa1-XN (0.42≤x<1), *Applied physics letters*, 2002, **81**:1255 [Crossref], [Google scholar], [Publisher]
[30]. Schmidt M.W., Baldridge K.K., Boatz J.A., Elbert S.T., Gordon M.S., Jensen J.H., Koseki S., Matsunaga N., Nguyen K.A., Su S., Windus T.L., Dupuis M., Montgomery Jr J.A., General atomic and molecular electronic structure system, *Journal of computational chemistry*, 1993, **14**:1347 [Crossref], [Google scholar], [Publisher]
[31]. Walker M., Harvey A.J.A., Sen A., Dessent C.E.H., Performance of M06, M06-2X, and M06-HF density functionals for conformationally flexible anionic clusters: M06 functionals perform better than B3LYP for a model system with dispersion and ionic hydrogen-bonding interactions, *The Journal of Physical Chemistry A*, 2013, **117**:12590 [Crossref], [Google scholar], [Publisher]
[32]. Rostami Z., Hosseinian A., Monfared A., DFT results against experimental data for electronic properties of C60 and C70 fullerene derivatives, *Journal of Molecular Graphics and Modelling*, 2018, **81**:60 [Crossref], [Google scholar], [Publisher]
[33]. Kazemi M., Rad A.S., Sulfur mustard gas adsorption on ZnO fullerene-like nanocage: Quantum chemical calculations, *Superlattices and Microstructures*, 2017, **106**:122 [Crossref], [Google scholar], [Publisher]
[34]. Deng WQ., Xu X., Goddard W.A., New alkali doped pillared carbon materials designed to achieve practical reversible hydrogen storage for transportation, *Physical review letters*, 2004, **92**:166103 [Crossref], [Google scholar], [Publisher]
[35]. Sedighi S., Baei M.T., Javan M., Ince J.C., Soltani A., Jokar M.H., Tavassoli S., Adsorption of sarin and chlorosarin onto the Al12N12 and Al12P12 nanoclusters: DFT and TDDFT calculations, *Surf Interface Anal*, 2020, **52**:725 [Crossref], [Google scholar], [Publisher]
[36]. Moghadami R., Vessally E., Babazadeh M., Es'haghi M., Bekhradnia A., Electronic and Work Function-Based Sensors for Acetylsalicylic Acid Based on the AlN and BN Nanoclusters: DFT Studies, *Journal of Cluster Science*, 2019, **30**:151 [Crossref], [Google scholar], [Publisher]
[37]. Mohammadi R., Hosseinian A., Khosroshahi E.S., Edjlali L., Vessally E., DFT study on the adsorption behavior and electronic response of AlN nanotube and nanocage toward toxic halothane gas, *Physica E: Low-dimensional Systems and Nanostructures*, 2018, **98**:53 [Crossref], [Google scholar], [Publisher]
[38]. Hoseininezhad-Namin M.S., Rahimpour E., Aysil Ozkan S., Pargolghasemi P., Jouyban A., Sensing of carbamazepine by AlN and BN nanoclusters in gas and solvent phases: DFT and TD-DFT calculation, *Journal of Molecular Liquids*, 2022, **353**:118750 [Crossref], [Google scholar], [Publisher]
[39]. Li J., Lu Y., Ye Q., Cinke M., Han J., Meyyappan M., Carbon nanotube sensors for gas and organic vapor detection, *Nano letters*, 2003, **3**:929 [Crossref], [Google scholar], [Publisher]

HOW TO CITE THIS ARTICLE
Mahdi Mohammad Alizadeh, Farshid Salimi, Gholamreza Ebrahimzadeh-Rajaei. Investigation of Adsorption Properties of $Al_{12}N_{12}$, $SiAl_{11}N_{12}$, and GaAl11N12 Nanoclusters for Sarin Detection: A Comparative DFT Study. *Chem. Methodol.*, 2023, 7(3) 248-256
https://doi.org/10.22034/CHEMM.2023.370868.1628
URL: http://www.chemmethod.com/article_163575.html